

Rheological, *In Situ* Printability and Cell Viability Analysis of Hydrogels for Muscle Tissue Regeneration

Srikanthan Ramesh¹, Sam Gerdes², Sharon Lau¹, Azadeh Mostafavi², Zhenyu (James) Kong³,
Blake N. Johnson³, Ali Tamayol², Prahalada Rao², Iris V. Rivero⁴

¹Department of Industrial and Manufacturing Systems Engineering, Iowa State University,
Ames, IA 50011

²Department of Mechanical and Materials Engineering, University of Nebraska, Lincoln, NE
68588

³Department of Industrial and Systems Engineering, Virginia Tech, Blacksburg, VA 24060

⁴Department of Industrial and Systems Engineering, Rochester Institute of Technology,
Rochester, NY 14623

Correspondence to: I. V. Rivero (E-mail: iris.rivero@rit.edu) and P. Rao (E-mail: rao@unl.edu)

Abstract

Advancements in additive manufacturing have made it possible to fabricate biologically relevant architectures from a wide variety of materials. Hydrogels have garnered increased attention for the fabrication of muscle tissue engineering constructs due to their resemblance to living tissue and ability to function as cell carriers. However, there is a lack of systematic approaches to screen bioinks based on their inherent properties, such as rheology, printability and cell viability. Furthermore, this study takes the critical first-step for connecting in-process sensor data with construct quality by studying the influence of printing parameters. Alginate-chitosan hydrogels were synthesized and subjected to a systematic rheological analysis. *In situ* print layer photography was utilized to identify the optimum printing parameters and also characterize the fabricated three-dimensional structures. Additionally, the scaffolds were seeded with C2C12 mouse myoblasts to test the suitability of the scaffolds for muscle tissue engineering. The results from the rheological analysis and print layer photography led to the development of a set of optimum processing conditions that produced a quality deposit while the cell viability tests indicated the suitability of the hydrogel for muscle tissue engineering applications.

Keywords: Printability; muscle regeneration; *in-situ* monitoring; bioprinting; C2C12 myoblasts

1. Introduction

Muscle tissues, being multi-functional, play a significant role in ensuring the general well-being of an individual.¹ In the event of severe damage to muscle tissues, medical mediation is often required to restore the quality of life of the patient. For example, volumetric muscle loss (VML), the traumatic or surgical loss of muscle with resultant functional impairment, is a debilitating condition that requires surgical intervention.² Currently, the gold standard for treating VML involves replacing the lost or damaged tissue with healthy and well-vascularized muscle tissue from outside the zone of injury. Although surgical techniques such as functional free muscle transfer (FFMT) and composite tissue allotransplantation (CTA) have been revolutionary and life-

saving, practical and medical limitations such as long operative times, availability of donors, donor site morbidity, and chronic immunosuppression have prompted the search for an engineered regenerative approach using scaffolds to restore the structure and function of the damaged tissue.³

Success in engineering scaffolds for muscle tissue regeneration is primarily determined by the capability to address two key challenges: firstly, the ability to identify and utilize materials that would satisfy the mechanical, chemical and biological demands of the tissue and secondly, the capability to fabricate a biologically relevant structure capable of mimicking the intricate architecture of the natural tissue. Since the advent of additive biofabrication techniques, subsequent developments in the field have mainly focused on developing systems that would enable the fabrication of complex three-dimensional structures. Today, it is possible to fabricate almost any complex bio-inspired geometry with a reasonable resolution and fidelity. For example, Sinton et al. reported the successful fabrication and biological evaluation of complex vasculature-like structures using an extrusion-based system.⁴ Another research team successfully printed and tested anatomically shaped cartilage structures using a 3D-bioprinter system equipped with a microvalve dispenser.⁵ Recently, Warner et al. designed and printed complex structures that exhibit fractal geometries using maskless stereolithography.⁶ The ability to repeatably reproduce such structures takes us a step closer to mimicking the internal architectures of organs such as the liver, lungs and the human retina.⁷⁻⁹ Over the last decade, a significant amount of progress has also been achieved in broadening the spectrum of materials compatible with additive biofabrication techniques such as extrusion-based printing, inkjet printing, laser-based printing, etc..^{10,11} As a result, a wide range of materials has either been developed or identified to be utilized in specific applications based on their physical, chemical and biological properties. For example, thermoplastic polymers are commonly preferred for fabricating scaffolds for bone tissues while hydrogels have been the preferred choice while aiming to regenerate softer tissues. Metals and bio-ceramics are also being increasingly used in manufacturing implants for dental and orthopedic applications.^{12,13} At this point where the fabrication of complex structures and availability of materials is no longer a major hurdle, it is our opinion that the focus of research in this field needs to be on developing strategies and protocols to ensure a smooth transition from laboratory-scale production to higher volumes of production without compromising repeatability.

In this study, hybrid hydrogels comprising of chitosan and sodium alginate were developed and evaluated for rheological behavior, and the optimum combination of process parameters was identified to achieve repeatable results. Two factors were considered before assessing the printability of the hydrogels: firstly, the ability of the gel to form strands with diameters resembling the diameter of the printing nozzle and secondly, the ability of the primary layer to support subsequent layers without the loss of shape fidelity due to the merging of the layers. *In situ* print-layer photography was used to capture images of the hydrogel strands during the printing process. The photographs were then used to assess the quality of the printed constructs using image processing techniques. Additionally, the cellular adhesion properties of the 3D-bioprinted structures were measured qualitatively and quantitatively using C2C12 mouse myoblast cells. In conclusion, this study provides a systematic approach to screen hydrogels based on rheology, printability and cellular viability.

2. Materials and Methods

2.1. Materials

Chitosan (CAS Number: 9012-76-4; Molecular Weight: 190000-375000 Da) extracted from shrimp shells, was purchased from Sigma Aldrich (St. Louis, MO) and used without further processing or purification. Acetic acid (CAS Number: 64-19-7; $\geq 99.85\%$) and sodium alginate (CAS Number: 9005-38-3) were also purchased from Sigma Aldrich (St. Louis, MO) and used as-received. Calcium chloride (CAS Number: 10043-52-4; Granular $\geq 93\%$) was obtained from Sigma Aldrich (St. Louis, MO) while sodium hydroxide (CAS Number: 1310-73-2; 97%) was purchased from Alfa Aesar (Ward Hill, MA).

2.2. Hydrogel Preparation

Hybrid hydrogels were prepared by dissolving chitosan and alginate with 1% (v/v) acetic acid in 10mM phosphate buffered saline solution and magnetically stirring for 3 hours at 45° Celsius. The hydrogel solutions were sealed using a parafilm while stirring to avoid external exposure. The three different formulations of hybrid hydrogels were as follows: (HH1) 3% (w/v) chitosan + 1% (w/v) sodium alginate, (HH2) 3.5% (w/v) chitosan + 0.75% (w/v) sodium alginate, (HH3) 4% (w/v) chitosan + 0.5% (w/v) sodium alginate. 2% (w/v) calcium chloride and 1% (w/v) sodium hydroxide were homogeneously mixed in deionized water and used as the cross-linking agent.

2.3. Rheological Measurements

Rheological measurements were obtained using an ARES-G2 rotational rheometer from TA Instruments (New Castle, DE). Two different routines were performed to fully understand the rheological behavior of the hydrogels. The first test was a steady shear sweep test intended to study the influence of shear stress (Pa) and shear rate (s^{-1}) on the viscosity (Pa.s) of the hydrogels. Curve fitting was then used to compute the power law index, n (dimensionless). The relationship between viscosity and shear rate is as shown below,

$$\eta = m\dot{\gamma}^{n-1} \quad [1]$$

where η , m , $\dot{\gamma}$, and n represents the viscosity, consistency index, shear rate and the power law index respectively.

The second test was a 3-phase thixotropic test with the hydrogels being subjected to the application of shear rate periodically. The first phase lasted for 30 s with a shear rate of $0.1 s^{-1}$ (low), the second for 30 s with a shear rate of $200 s^{-1}$ (high) and the third for 30 s with a low shear rate again. The change in viscosity was plotted as a function of time, and the viscosity recovery behavior of the hydrogels was analyzed. The second study was designed to resemble the actual printing process which involves the periodic application of low and high shear rates.

2.4. Three-dimensional Bioprinting

Three-dimensional bioprinting was carried out using the 3D-Bioplotter (manufacturer series) from EnvisionTEC (Gladbeck, Germany). The bioplotter allowed the manipulation of process parameters such as printing pressure, holding temperature, print bed temperature, horizontal translational speed, infill pattern, pre-flow, post-flow, needle offset, and needle size to optimize

the print quality and structural stability of the printed constructs. The hydrogels were extruded pneumatically into Petri dishes before adding the cross-linking agent using a syringe. An onboard camera was utilized to capture photographs of several locations on the build-platform after the completion of each layer. Process parameters such as printing pressure (bar), printing speed (mm/s) and printhead temperature (°C) were varied, and their effects studied. Other process parameters such as nozzle diameter (21G; 0.8 mm) print bed temperature (°C), needle offset (mm), pre-flow (0.05 s), and post flow (-0.05 s) were held constant.

2.5. Line Width Assessment

Linear print speed was optimized based on the printing pressure by utilizing the onboard camera and line width analysis software. For this analysis, three pressures (0.2-0.4 bar) and three printhead temperatures (6, 12, and 18 °C) at which the hydrogel was printable was selected, and lines were printed at five different speeds (26-30 mm/s) for each pressure and temperature setting. After the lines were given several minutes to crosslink, the line widths were recorded by the onboard camera.

2.6. Scaffold Fabrication and Print Quality Assessment

Once the optimum process parameters were identified, three-dimensional scaffolds with 0-90° strand orientation were printed, and quality tested for percentage porosity and circularity of the pores using image processing techniques. The circularity values of the pores were calculated using the following equation,

$$C = \frac{4\pi \cdot A}{(P)^2} \quad [2]$$

where C (dimensionless), A (mm²) and P (mm) represent the circularity, area, and perimeter of the pores.

2.7. Cellular Viability Evaluation

C2C12 mouse myoblasts were cultured on the scaffolds to assess biocompatibility. The hydrogel scaffolds were washed with phosphate buffered saline (PBS) followed by sterilizing them with 1% penicillin-streptomycin. Cells were seeded on scaffolds (2 ×10⁴ cells for live/dead assay and 10⁴ cells for PrestoBlue[®] assay) and evaluated at different time points. Cell viability was determined with Live/Dead staining (LIVE/DEAD[®] Viability/Cytotoxicity Kit, L3224, Invitrogen, USA) at the end of 24 hours. Scaffolds were then washed with PBS and stained with a solution of 2 μL ethidium homodimer-1 and 0.5 μL of calcein in PBS for 30 minutes and incubated at 37 °C. Cells were then imaged with a fluorescent microscope (Nikon) with TRITC and FITC filters to detect ethidium homodimer-1 (Ex/Em 528/617 nm) and calcein (Ex/Em 528/617 nm) respectively. The metabolic activity was assessed by PrestoBlue[®] assay at days 1, 3, and 7. Cultured cells on scaffolds were incubated with 10 % (v/v) solution of PrestoBlue[®] (Cell viability Reagent, A13262, Invitrogen, USA) for 1 hour. Then, 100 μL of the solution was transferred in a 96-well plate, and fluorescence (Ex/Em 535/615 nm) was measured by a Multi-Mode Reader (BioTek, Winooski, VT). Cells cultured on tissue culture plate were used as the control.

3. Results and Discussion

3.1. Rheological Measurements

Hydrogels for bioprinting must satisfy some crucial requirements to enable the repeatable creation of three-dimensional architectures. Out of all the needs, rheological behavior holds utmost importance as it determines the printability of a material. Measurements of routine rheological properties such as yield stress, viscosity as a function of shear rate, and viscosity recovery behavior of a hydrogel can be used to derive a preliminary idea of the flow behavior of a liquid.

In this study, a shear ramp was used to obtain a plot of viscosity as a function of the shear stress of the developed hydrogels, this plot is shown in Figure 1(a). The yield stress of each hydrogel allows the identification of yield stress which describes the point below which a material behaves like a solid and above which flows like a liquid.¹⁴ By qualitatively looking at the plot, a clear distinction can be made between printable (HH1, HH2) and unprintable materials (HH3). For instance, the hybrid hydrogel comprising of the highest loading of chitosan did not show a significant drop in viscosity at any point during the shear ramp indicating an inability to flow consistently under the application of shear stress. In contrast, both hydrogels HH1 and HH2 displayed distinct points after which the viscosity of the material dropped significantly indicating a tendency to flow. However, HH1 showed lower levels of viscosity than HH2 at all times during the shear ramp and hence was the preferred choice.

A second plot, Figure 1(b), showing the changes in viscosity as a function of shear rate was used to characterize the shear thinning behavior of the hydrogels. The linear region of the double-logarithm plot was modeled using power law to quantitatively describe the shear thinning behavior of the hydrogels. As shown in Table 1, all the hydrogels exhibited shear thinning behavior as all the power law indices recorded were lesser than 1.

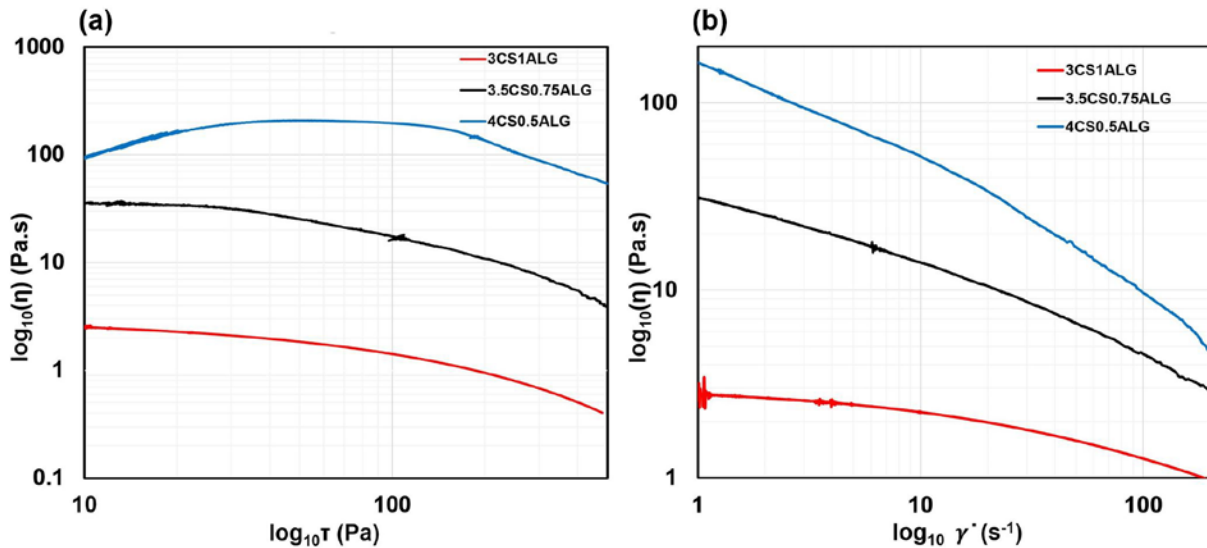


Figure 1. The plot of hydrogel viscosity as a function of (a) shear stress and (b) shear rate.

Table 1. Power law indices obtained via curve fitting.

Hydrogel	Power Law Index
3CS1ALG (HH1)	0.8
3.5CS0.75ALG (HH2)	0.6
4CS0.5ALG (HH3)	0.3

Finally, the viscosity recovery capabilities of the hydrogels were quantified using a three-phase thixotropic test and displayed in Figure 2. The net loss in viscosity was calculated for each hydrogel and presented in Table 2. It was evident that HH1 exhibited the least overall decline in viscosity indicating the ability of the material to rapidly increase its viscosity after the removal of shear rate enabling the maintenance of the fidelity of the deposited structures. Based on the results from all the rheological tests conducted, HH1 was chosen as the ideal material to develop scaffolds repeatably. Even though the shear-viscosity measurements do not adequately characterize the flow behavior of liquids as they do not consider other factors such as surface tension and dynamic viscoelastic properties, they help form the foundation required to understand the printability of these materials.¹⁵

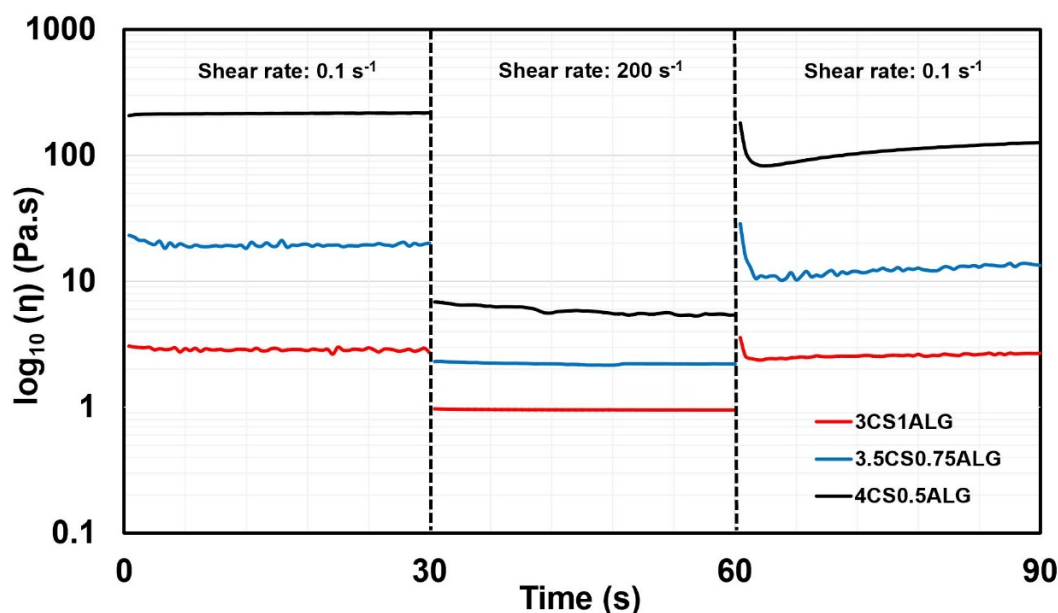


Figure 2. Plot describing viscosity as a function of time at constant shear rates (0.1 s^{-1} and 200 s^{-1}).

Table 2. Net loss in viscosity of the hydrogels after the application of alternating shear rates.

Hydrogel	Net Loss in Viscosity (%)
3CS1ALG (HH1)	0.3
3.5CS0.75ALG (HH2)	5.5
4CS0.5ALG (HH3)	1.8

3.2. Line Width Assessment

Singular strands were deposited to monitor the dimensional accuracy and shape fidelity of the deposition. Based on these criteria, the optimum pressure, printing speed, and printhead temperature were chosen to bioprint scaffolds. The photographs taken using the onboard camera are shown in Figure 3, and the observed relationships between strand width and process parameters are described in Figure 4.

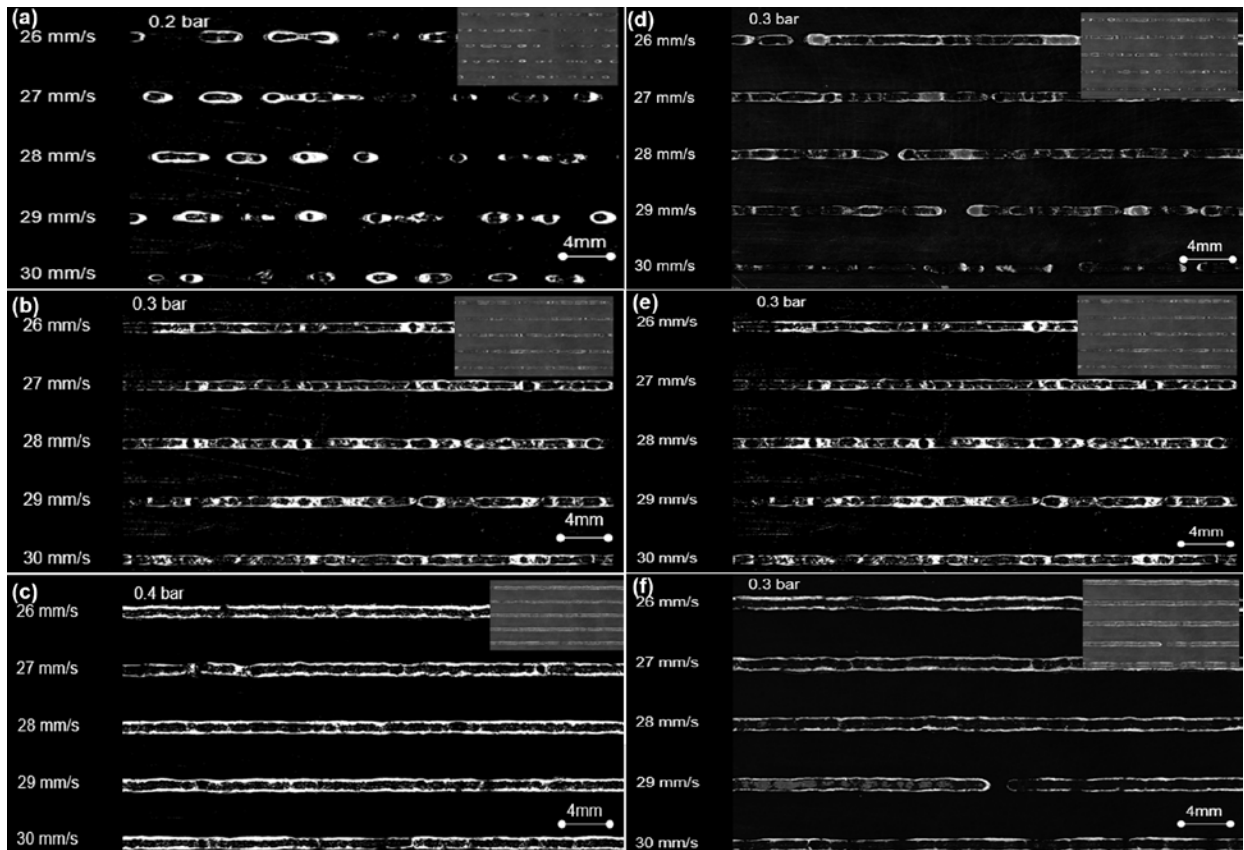


Figure 3. Photographs of singular strands deposited at (a) 0.2 bar, 12 °C; (b) 0.3 bar, 12 °C; (c) 0.4 bar, 12 °C; (d) 0.3 bar, 6 °C; (e) 0.3 bar, 12 °C; (f) 0.3 bar, 18 °C. At each pressure-temperature, strands were deposited at five different speeds (26 mm/s – 30 mm/s).

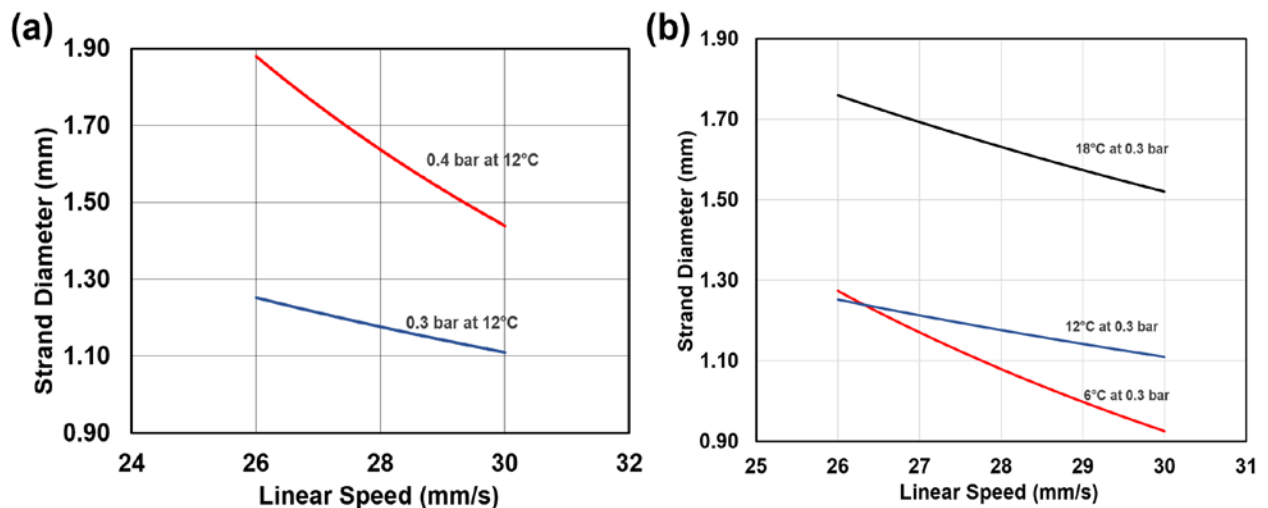


Figure 4. Plot describing the influence of (a) pressure-speed relationship on strand width and (b) temperature-speed relationship on strand diameter.

It was observed that increasing the printing pressure increases the strand diameter; it is hypothesized that the underlying reason is the increase in the material flow rate.¹⁶ Temperature

testing indicated a rise in strand width with increasing temperature, as well as, reduced fidelity especially in the case of the lowest temperature tested. Similar trends have been reported in the literature during the printing of GelMA, and it has been attributed to a decrease in the tightness of the crosslinked polymeric structure with increasing temperatures.¹⁷ Consequently, it was hypothesized that an increase in temperature decreased the attraction between chitosan and alginate resulting in the reduction of viscosity. In both the pressure and temperature analyses, increased print speed decreased average strand width. However, in the low pressure and low-temperature cases, increased print speed led to broken strands. This was due to an extrusion rate which could not provide sufficient volume to create a consistent strand at a constant print speed.

3.3. Scaffold Fabrication and Print Quality Assessment

The generation of pores in a bioprinted scaffold is hugely crucial to the utility of the scaffold. Percentage porosity and the pore size play a critical role as they allow the attachment, migration, and proliferation of the myoblasts, as well as vascularization. The scaffolds were initially designed with a theoretical porosity of 70% and were intended to be square as seen in Figure 5(a). The photographs of bioprinted scaffolds shown in Figure 5(b) were subjected to digital image processing and analysis. It was observed that the bioprinted scaffold had an actual porosity of 68% Figure 5(c). Additionally, in an attempt to quantify the shape fidelity of the pores, mean circularity of the pores were calculated and estimated to be 0.72 Figure 5(d). It is to be noted that an ideal square possesses a circularity value of 0.78. In conclusion, the bioprinted structures closely resembled the ideal three-dimensional design of the scaffold.

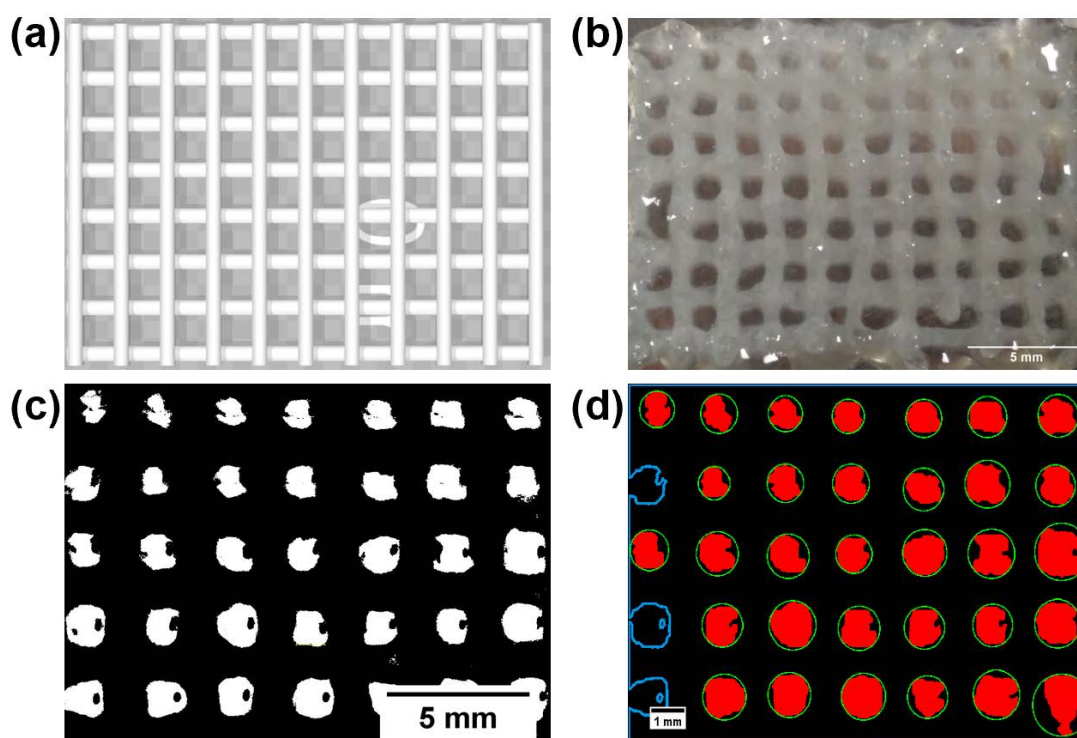


Figure 5. Representative images showing (a) theoretical scaffold design (b) bioprinted and crosslinked scaffold made of 3% chitosan and 1% alginate hydrogel (c) binary image of the scaffold to assist in the visualization of porosity (d) the result of contour detection performed on a thresholded photograph of the bioprinted scaffold.

3.4. Cell Viability Analysis

To assess the biocompatibility of the fabricated scaffolds and verify their effectiveness in supporting cellular growth, C2C12 cells were seeded on the bioprinted hydrogel scaffolds. Cellular viability and metabolic activity were assessed using the LIVE/DEAD[®] Assay Kit and PrestoBlue[®] assay, respectively. The results from the LIVE/DEAD assay showed high cellular viability (shown in green) on the scaffolds and limited toxicity (dead cells shown in red) at the end of day 1 (Figure 6). The metabolic activity of cells was evaluated and compared to the control by using PrestoBlue[®] assay after 1, 3 and 7 days of culture. The results verified the observations from the LIVE/DEAD assay and indicated a proliferation rate compared to the control group with negligible toxicity (Figure 7).

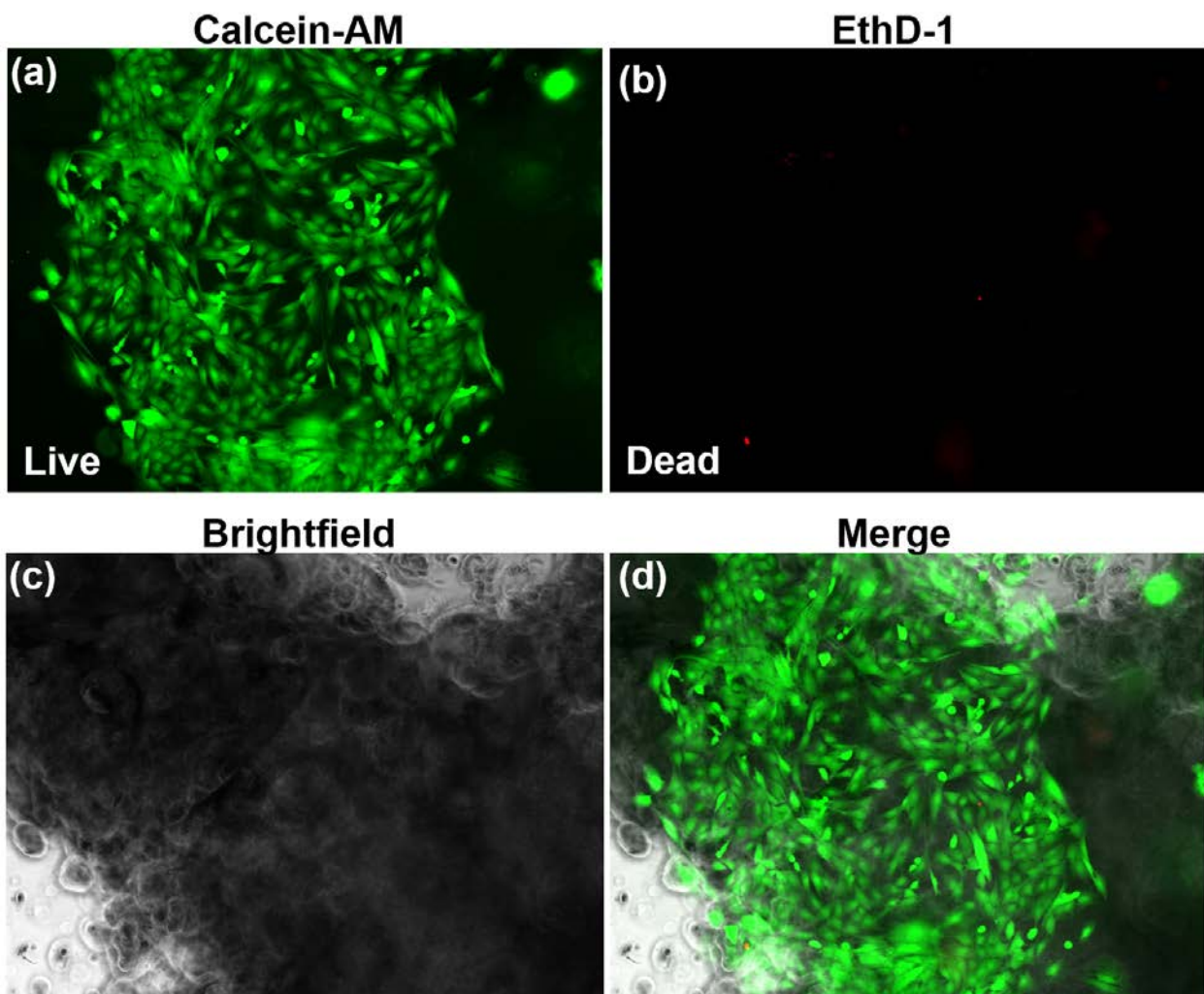


Figure 6. Representative micrographs of C2C12 mouse myoblasts seeded on chitosan-alginate scaffolds for 24 hours. (a) live cells (shown in green), (b) dead cells (shown in red), (c) Brightfield, and (d) merged.

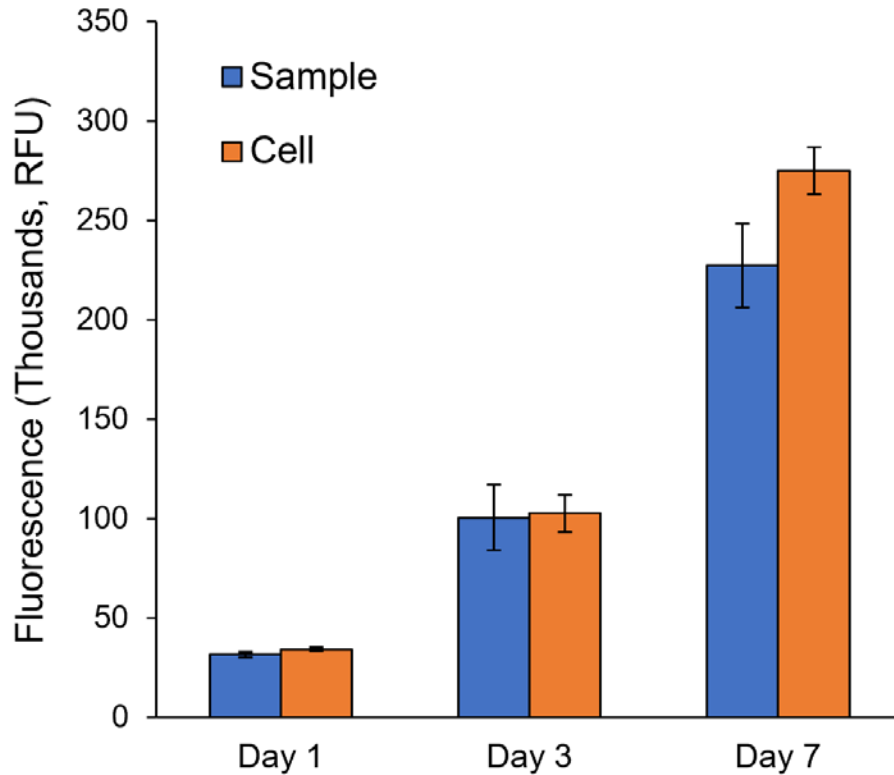


Figure 7. Results of PrestoBlue® shows metabolic activity and cell proliferation of cells seeded on bioplotted scaffolds in comparison to the control at various time points (1, 3, and 7 days).

4. Conclusions

This study provided a systematic approach to screen hydrogels based on rheological behavior followed by a methodical optimization to identify process parameters to facilitate the repeatable deposition of a hydrogel in a cross-linking medium. The results of this study can be concluded as follows,

- Based on its shear thinning and viscosity recovery behavior, 3% (w/v) chitosan + 1% (w/v) alginate hydrogel was identified to be suitable for biplotting
- *In situ* visual inspection indicated the strand diameter had a directly proportional relationship with printing pressure and an inversely proportional relationship with printing speed.
- The shape fidelity of pores and percent porosity values of the bioplotted scaffold resembled that of the theoretical three-dimensional design validating the robustness of the process.
- The attachment and proliferation of C2C12 mouse myoblasts on the bioplotted scaffolds confirmed biocompatibility with negligible toxicity.

Acknowledgments

The authors (PR, ZK, BJ, SG) thank the NSF for funding this work through the following award and ensuing research experience for undergraduates (REU) supplement, CMMI 1739696 entitled CPS: Medium: Collaborative Research: Cyber-Enabled Online Quality Assurance for Scalable Additive Bio-Manufacturing. The sensing and monitoring approach described in this work was an integral part of the grant mentioned above. The authors would also like to extend their thank the Nano-Engineering Research Core Facility (NERCF), University of Nebraska, Lincoln and the Department of Chemical and Biological Engineering, Iowa State University for providing access to the bioprinter and rheometer respectively.

References

- (1) Lindstedt, S. L. Skeletal Muscle Tissue in Movement and Health: Positives and Negatives. *J. Exp. Biol.* **2016**.
- (2) Sicari, B. M.; Agrawal, V.; Siu, B. F.; Medberry, C. J.; Dearth, C. L.; Turner, N. J.; Badylak, S. F. A Murine Model of Volumetric Muscle Loss and a Regenerative Medicine Approach for Tissue Replacement. *Tissue Eng. Part A* **2012**.
- (3) Levenberg, S.; Rouwkema, J.; Macdonald, M.; Garfein, E. S.; Kohane, D. S.; Darland, D. C.; Marini, R.; Van Blitterswijk, C. A.; Mulligan, R. C.; D'Amore, P. A.; et al. Engineering Vascularized Skeletal Muscle Tissue. *Nat. Biotechnol.* **2005**.
- (4) Suntornnond, R.; Tan, E. Y. S.; An, J.; Chua, C. K. A Highly Printable and Biocompatible Hydrogel Composite for Direct Printing of Soft and Perfusable Vasculature-like Structures. *Sci. Rep.* **2017**.
- (5) Markstedt, K.; Mantas, A.; Tournier, I.; Martínez Ávila, H.; Hägg, D.; Gatenholm, P. 3D Bioprinting Human Chondrocytes with Nanocellulose-Alginate Bioink for Cartilage Tissue Engineering Applications. *Biomacromolecules* **2015**.
- (6) Warner, J.; Soman, P.; Zhu, W.; Tom, M.; Chen, S. Design and 3D Printing of Hydrogel Scaffolds with Fractal Geometries. *ACS Biomater. Sci. Eng.* **2016**.
- (7) Vozzi, G.; Previti, A.; Ciaravella, G.; Ahluwalia, A. Microfabricated Fractal Branching Networks. *J. Biomed. Mater. Res. - Part A* **2004**.
- (8) Masters, B. R. Fractal Analysis of the Vascular Tree in the Human Retina. *Annu. Rev. Biomed. Eng.* **2004**.
- (9) Hayashi, T.; Carthew, R. W. Surface Mechanics Mediate Pattern Formation in the Developing Retina. *Nature* **2004**.
- (10) Jungst, T.; Smolan, W.; Schacht, K.; Scheibel, T.; Groll, J. Strategies and Molecular Design Criteria for 3D Printable Hydrogels. *Chemical Reviews*. 2016.
- (11) Murphy, S. V.; Atala, A. 3D Bioprinting of Tissues and Organs. *Nat. Biotechnol.* **2014**, 32 (8), 773–785.
- (12) Dawood, A.; Marti, B. M.; Sauret-Jackson, V.; Darwood, A. 3D Printing in Dentistry. *Br. Dent. J.* **2015**.
- (13) Habibovic, P.; Gbureck, U.; Doillon, C. J.; Bassett, D. C.; van Blitterswijk, C. A.; Barralet, J. E. Osteoconduction and Osteoinduction of Low-Temperature 3D Printed Bioceramic Implants. *Biomaterials* **2008**.
- (14) Coussot, P. Yield Stress Fluid Flows: A Review of Experimental Data. *Journal of Non-Newtonian Fluid Mechanics*. 2014.
- (15) Paxton, N.; Smolan, W.; Böck, T.; Melchels, F.; Groll, J.; Jungst, T. Proposal to Assess Printability of Bioinks for Extrusion-Based Bioprinting and Evaluation of Rheological

- Properties Governing Bioprintability. *Biofabrication* **2017**.
- (16) Kang, K. H.; Hockaday, L. A.; Butcher, J. T. Quantitative Optimization of Solid Freeform Deposition of Aqueous Hydrogels. *Biofabrication* **2013**.
- (17) Kolesky, D. B.; Truby, R. L.; Gladman, A. S.; Busbee, T. A.; Homan, K. A.; Lewis, J. A. 3D Bioprinting of Vascularized, Heterogeneous Cell-Laden Tissue Constructs. *Adv. Mater.* **2014**.